WILEY-VCH

Advanced Materials
DOI: 10.1002/((please add manuscript number))
Article type: Communication

Ultra-low power optical synapses based on MoS_2 layers with indium-induced surface charge doping for biomimetic eyes

*Yunxia Hu, Mingjin Dai, Wei Feng, Xin Zhang, Feng Gao, Shichao Zhang, Biying Tan, Jia Zhang, Yong Shuai, YongQing Fu, PingAn Hu**

((Optional Dedication))

Y. Hu, F. Gao, Prof. P. Hu
School of Materials Science and Engineering
Harbin Institute of Technology
Harbin 150001, China
E-mail: hupa@hit.edu.cn

Y. Hu, X. Zhang, F. Gao, S. Zhang, B. Tan, J. Zhang, Prof. P. Hu
MOE Key Laboratory of Micro-Systems and Micro-Structures Manufacturing
Harbin Institute of Technology
Harbin 150001, China

Dr. M. Dai
School of Electrical and Electronic Engineering
Nanyang Technological University
Singapore 639798, Singapore

Dr. W. Feng
Department of Chemistry and Chemical Engineering
College of Science
Northeast Forestry University
Harbin 150040, China

Prof. Y. Shuai
School of Energy Science and Engineering
Harbin Institute of Technology
Harbin 150001, China

Prof Y.Q. Fu (Richard)
Faculty of Engineering & Environment
Northumbria University
Newcastle upon Tyne, NE1 8ST, United Kingdom

Keywords: synaptic devices, MoS_2, ultra-low power consumption, biomimetic eyes, image learning

Biomimetic eyes, with their excellent imaging functions such as large fields of view and low aberrations, have shown great potentials in the fields of visual prostheses and robotics. However, high power consumption and difficulties in device integration severely restrict their rapid development. In this study, an artificial synaptic device consisting of a MoS_2 film coated with an electron injection enhanced indium layer is proposed to increase the channel conductivity and reduce the power consumption. This artificial synaptic device achieves an ultra-low power consumption of 68.9 aJ per spike, which is several hundred times lower than those of the optical artificial synapses reported in literature. Furthermore, the multilayer and polycrystalline MoS_2 film shows persistent photoconductivity (PPC) performance, effectively resulting in short-term plasticity (STP), long-term plasticity (LTP) and their transitions between each other. A 5 × 5 In/MoS_2 synaptic device array has been constructed into a hemispherical electronic retina, demonstrating its impressive image sensing and learning functions. This research provides a new methodology for effective control of artificial synaptic devices, which have great opportunities used in bionic retinas, robots and visual prostheses.

Main text

The eyes of arthropods, consisted of hemispherical retinas and optical components, are one of the most important sensory organs with excellent image sensing characteristics such as wide field of view, high resolution, high sensitivity and infinite depth of field.[1] Inspired by the biological eyes, biomimicry visual systems consisted of photodetectors, memory devices and processing units have recently been developed to realize image sensing functions.[2-7] However, current structures of these biomemetic visual systems are difficult used to perform complex tasks of image learning and processing (such as those in a biological vision system) and often consume a large amount of eletrical powers.[8-9] Therefore, multifunctional electronic devices which can integrate sensing and memory functions are urgently required for these biomemetic visual systems. Particularly, synaptic devices under the optical modulation can respond to the

optical stimuli and show a typical synaptic plasticity. They combine the visual systems and brain functions, exhibiting great prospects in artificial intelligence for image recognition and learning.[8, 10-11] However, rigid materials, complex device structures, and high power consumption of the current synaptic devices become critical issues for the rapid development of neural networks, and exploration of novel materials and synaptic devices is highly demanded.

Currently, artificial synapses based on silicon,[12] oxide films,[13-14] organic materials[15] and two dimensional (2D) inorganic materials[16-17] have been fabricated and shown synaptic plasticity. Particularly, 2D materials are considered as the outstanding candidates for the artificial optical synapses due to their unique atomic structures, mechanical flexibility and excellent optical and electrical properties. Among them, molybdenum disulfide (MoS_2), with its superb photoresponsivity,[18-19] high fracture strain[20-21] and well-developed preparation methods[22-26], has been widely investigated to mimic synaptic plasticity under an optical modulation. Several types of optical synapses, including TiN_xO_{2-x}/MoS_2 heterostructure[27] and MoS_2/PTCDA hybrid heterostructure,[28] have been proposed to perform optic-neural synaptic functions, and show good potentials in constructing human visual systems. However, the power consumption of these optical synapses based on MoS_2 is often hundreds of times higher than that of the biological synapses (≈10 fJ per activity), which is disadvantageous for their practical applications. The key reason is that the ultra-thin feature of 2D materials such as MoS_2 leads to difficulties of introducing dopants inside, thus restricting the precise control of electrical properties and modulation of power consumption of devices.

In this work, we design an artificial synaptic device based on MoS_2 film covered with an electron injection enhanced indium layer. Electrons in the indium layer can be injected into MoS_2 because the Fermi level of the indium is higher than that of MoS_2. This results in an effective increase of the channe's electrical conductivity and a signficant reduction of power consumption of the optical synapse down to 68.9 aJ per spike, which is much lower than those of the currently developed synaptic devices. Based on the inherent persistent photoconductivity

(PPC) performance of the MoS_2 film, the In/MoS_2 synapse devices have achieved essential synaptic functions including short-term plasticity (STP), long-term plasticity (LTP) and their transition between each other. Furthemore, a hemispherical electronic retina consisted of a 5×5 In/MoS_2 synaptic device array has been fabricated, exhibiting high performance image sensing and learning functions. This work opens up a new route to regulate the performance of synaptic devices based on the 2D materials and demonstrates their great prospects in artificial neuromorphic vision systems consisted of the hemispherical electronic retina.

Figure 1a provides schematic diagrams of the human visual system and biological synapses**.** The human visual system is consisted of (1) the eyes that collect light and convert it into electrical signals, (2) the visual cortex of the brain that processes data of the signals, and (3) the nerves that connect the eyes and the brain to transmit the data.[1, 29] Among them, synapses are the basic units of nerves for computing and memorizing various electrical signals. Figure 1a also shows a schematic diagram of the artificial synaptic device, which includes a MoS_2 film and a discontinuous indium layer. Figure 1b exhibits the fabrication processes of the In/MoS_2 synaptic device. Using, The synaptic devices with a two terminal configuration are fabricated on the MoS_2 synthesized from a chemical vapor deposition (CVD) covered with a discontinuous indium layer. Metal (Au) electrodes are further deposited onto the above structure using a thermal evaporation method.

An optical microscope image of the fabricated In/MoS_2 synaptic device is shown in Figure 1c. Figure 1d shows a scanning electron microscope (SEM) image of the indium layer deposited on the MoS_2 film. It can be clearly seen that the indium layer is not continuous and has its morphologies similar to triangles or hexagons attributed to the epitaxial effect of MoS_2 during the thermal deposition process. Raman spectrum of the MoS_2 film is shown in Figure 1e. The frequency difference between the E_{2g}^{1} peak and A_{1g} peak is more than 20 cm^{-1}, which indicates that the film is multilayer MoS_2.[30] Photoluminescence (PL) peak position of the MoS_2 is

located at 1.76 eV, further verifying that the MoS_2 film has a multilayer structure[31-32] (Figure S1). In addition, Figure S2 shows an image of MoS_2 film obtained using a tapping-mode atomic force microscope (AFM). It shows that the thickness of MoS_2 film synthesized on the quartz plate is about 3 nm.

To analyze the chemical composition of the MoS_2 film, its spectra of X-ray photoelectron spectroscope (XPS) are obtained and the results are shown in Figure S3. The binding energies of Mo $3d_{5/2}$ and Mo $3d_{3/2}$ are located at 229.4 and 232.5 eV (Figure S3a), and the peaks at 161.6 and 162.8 eV (Figure S3b) are corresponding to the binding energies of S $2p_{3/2}$ and $2p_{1/3}$, respectively. These results prove the formation of MoS_2. Figure S3c is the survey spectrum of the sample, showing that there is no other element in the MoS_2 film. Furthermore, result obtained using X-ray diffraction (XRD, Figure S4) confirms the crystalline structure of MoS_2 (JCPDS card no. 37-1492). Transmission electron microscope (TEM) is used to characterize the crystal quality of MoS_2 film. Figure S5a is a representative low-magnification TEM image, in which the MoS_2 film is formed by stacking many small MoS_2 crystals. From the high-resolution TEM (HRTEM) images of the internal and edge regions of the MoS_2 film (Figures S5b and S5d), we can confirm that the MoS_2 film has a polycrystalline and multi-layer structure. Selected area electron diffraction (SAED) pattern shown in Figure S5c further confirms the polycrystalline nature of the MoS_2 film.

In a neuronal system, presynaptic neurons release neurotransmitters to stimulate postsynaptic neurons, thus generating excitatory postsynaptic current (EPSC) when the neurotransmitters strengthen the synaptic transitions. Synaptic plasticity is an adjustable characteristic of the strength of neural connections. In a MoS_2 synapse device, the photon stimulus is regarded as a presynaptic spike, the conductance of the monolayer MoS_2 is considered as the synaptic weight, and the drain current of the device functionalizes as the postsynaptic current. Synaptic plasticity, the phenomenon that the channel current changes with the light illumination, can be imitated in the MoS_2 polycrystals due to their PPC effects.[33-34]

To explore the origin of the PPC effect in MoS_2 polycrystals, the PL spectral intensities of multilayer MoS_2 and monolayer MoS_2 are characterized and compared (Figure S1). The PL spectral intensity of multilayer MoS_2 is much lower than that of monolayer MoS_2, proving the existence of interlayer coupling in the multilayer MoS_2.[35] Furthermore, quantitative XPS analysis of the MoS_2 has been conducted. The obtained ratio of Mo/S in the MoS_2 is 1.07:1, which is much higher than 1: 2, demonstrating the formation of lots of sulfur vacancies in the MoS_2. Sulfur vacancies of MoS_2 has been reported as the deep-level defects, which result in the formation of PPC effects in the MoS_2 device.[36-37] When the visible light stimulates the MoS_2 device, photogenerated electron-hole pairs are produced, whereas the interlayers and defects of multilayer MoS_2 can restrict the rapid recombination between the electrons and holes. Therefore, the channel currents in the MoS_2 device will not immediately disappear after the light is switched off. The trapping and gradual release of electrons simulate the changes of synaptic weight in the synapses, thus realizing optical synaptic functions in the MoS_2 devices.

Figure S6a shows a typical photo-response of the MoS_2 channel under the light illumination at 100 mV for 100 s. The relaxation time of the MoS_2 device exceeds 100 s, which proves the existence of PPC effect of this MoS_2 synaptic device. When the synapse device is stimulated by a light with a wavelength of 550 nm, the MoS_2 channel generates the electron-hole pairs. The electrons are trapped in the multilayer MoS_2 film and slowly released. This PPC effect also leads to the gradual increase of current with the increase of the illumination time. The channel current of the MoS_2 device is also increased when the light is switched on, which is due to the pyroelectric effect (e.g., caused by the light-induced heating and the elevated temperature of the device). When the temperature becomes stable, the pyroelectric effect disappears and the current returns to a stable value. Whereas the current will gradually decrease after switching off the light due to the PPC effect. At the moment of switching off the light, the device's temperature will suddenly drop and then return to a stable value, which results in a falling peak of the current.[38, 39] Results of ΔEPSC ($(I_{ph} - I_{dark}) / I_{dark}$), which is an important

indicator of the synaptic strength,[40] are shown in Figure S6b as a function of light duration. Here, I_{dark} is the dark current, I_{ph} is the photocurrent, and I_{ph} - I_{dark} is the current difference between the light illumination condition and the dark condition. The value of ΔEPSC increases with the increase of the light duration, which is due to the generation of more electron-hole pairs under a longer light duration, thus resulting in the significantly increased photocurrents. Figures S6c and S6d show the typical transient light response curves of the MoS_2 synaptic device with different numbers of light pulses (with the same pulse width of 50 ms and a pulse interval of 50 ms) at a voltage of 100 mV, and the corresponding ΔEPSC values as a function of light pulse number, respectively. As the number of light pulses increases, both the photo-responses and the values of ΔEPSC increase, which demonstrates the formation of synaptic plasticity in the MoS_2 synaptic device. This is because after the previously applied light pulse is off, the photogenerated electron-hole pairs are slowly recombined and thus there is still crurrent remained befrore switching the light again. This will result in the increased current values after the next light pulse is applied.

In addition to the light duration and the number of light pulses, the synaptic weight of the MoS_2 synaptic device can also be adjusted by the light intensity with a wavelength of 550 nm and a duration of 20 s (Figure S7a). The postsynaptic current (PSC) is much larger under a stronger light intensity. Therefore, the ΔEPSC value is positively correlated to the light intensity (Figure S7b). Furthermore, the pair-pulse-facilitation (PPF) phenomenon of the MoS_2 synaptic device has been explored in this work, and this is an important manifestation of the synaptic plasticity.[10, 14] When two identical pulses continuously stimulate synapses at short intervals, the increase of synaptic weight caused by the second spike is much larger than that caused by the first spike. This is due to the memory generation of the previous stimulation, even if the first spike has already been stopped. Figure S8a shows the PPF behavior of the MoS_2 synaptic device with an interval time of 2 s, an excitation wavelength of 550 nm and a voltage of 100 mV. It is clear that the second PSC (A_2) is higher than the first one (A_1). The facilitation ratio

(a PPF index [10] which is the ratio between the amplitudes of A_2 and A_1) can quantitatively indicate the synaptic strength. Figure S8b shows the obtained PPF index as a function of interval time. The smaller the interval time between these two light pulses is, the larger the PPF index is, demonstrating that a shorter time interval is beneficial to the post-synaptic facilitation. In a biological synapse, the Ca^{2+} concentration after the second spike in the pre-synaptic neuron is much larger due to the Ca^{2+} residue generated after the first spike, thus inducing the PPF phenomenon.[41] Similar to the biological synapses, the PPF in the MoS_2 synaptic device is associated with the slow recombination process of photo-generated carriers, due to the existence of multi-layers and defects in the MoS_2 film. When the second light pulse is applied during the relaxation time of the first light pulse, the PSC index will be larger than 100%.

Although the conventional MoS_2 synaptic device exhibits an excellent synaptic plasticity, its energy consumption is generally quite large, e.g., more than 1 pJ.[27-28, 42] This is much larger than the power consumption of synapses in the biological systems, thus restricting its practical applications. The surface charge transfer doping strategy based on the application of an indium layer in this study has significantly reduced the power consumption of the artificial synapses device, because it can decrease the applied voltage under the same current magnitude.[43-44] The corresponding schematic diagram of this energy reduction mechanism is illustrated in Figure 2a. Not only can the discontinuous indium layer be used as a protective layer of the MoS_2 and enhance the contact between the MoS_2 and electrodes, but also a large number of electrons in the discontinuous indium layer will be injected into the MoS_2, thus significantly increasing the conductivity of the material.

Figure 2b illustrates the energy-band alignment between the two layers of MoS_2 and indium. When these two materials are not in contact, the Fermi level (E_f) of indium is higher than the conduction band (E_c) of the MoS_2, because the work function of indium (4.1 eV) is lower than that of the MoS_2 (4.7 eV).[43, 45] The difference of E_f causes the electrons in the indium layer to flow into the MoS_2 when they are contact with each other until the E_f becomes

an equilibrium. This will result in the downward bending of E_c and the accumulation of electrons in MoS_2. Therefore, the conductivity of the MoS_2 device deposited with an indium layer is significantly larger than that without an indium layer. Moreover, the junction between indium and MoS_2 can make electrons to flow easily between each other, which leads to the formation of a good ohmic contact at the interfaces between indium and MoS_2.

Figure 2c shows the results of EPSC for the MoS_2 device covered by an indium layer with a surface coverage of 55% and a voltage of 100 mV, but with different light exposure durations. Compared with that of MoS_2 synaptic devices, the current of 55% In/MoS_2 ones can be increased by about 1000 times, demonstrating that the electrons have been effectively transferred from the indium layer to MoS_2. The psychological memory and forgetting model of a human brain was previously proposed by Atkinson and Shiffrin,[46-47] and is shown in Figure S9. The existence of STP and LTP as well as the effective transition between each other are crucial foundations of the psychological memory and forgetting models of a human brain. Among them, the STP is the synaptic plasticity with a temporary potentiation which lasts for a few seconds or minutes. The potentiation before the LTP is recovered to its original state can be maintained for more than 100 seconds. In the human brain, the sensory information stored in the sensory memory can be converted into the STP, and frequent practices or enhanced stimulation can transform the STP into the LTP, thus achieving the adjustability of neuronal synaptic plasticity and the formation of synaptic learning and memory. To imitate the rehearsal in the human brain, the currents of the In/MoS_2 device with the light durations increased from 5 s to 100 s are measured and the obtained results are shown in Figure 2c. The recombination times of photo-generated electron-hole pairs have been increased from about ten seconds to hundreds of seconds by increasing the light duration from 5 s to 100 s, which demonstrates the transition from the STP to LTP in the In/MoS_2 synaptic device by increasing the light duration. Figure 2d shows the ΔEPSC results as a function of duration time at 100 mV. Due to the time-

dependent photo-generated carriers, the synapse weight changes significantly with the prolonged light duration.

To imitate the instantaneous information transmission in the biological synapses, the synaptic responses of the In/MoS_2 device under a short light pulse stimulus (50 ms) has been measured, and the results are shown in Figure 2e. The obvious changes of channel currents and the memory time of about 2 s under the optical pulse prove the functions of instantaneous information detection and memory generation from the synaptic devices. Furthermore, the increase in the number of light pulses is linked to the increased rehearsals of the optical stimuli. Figure 2f exhibits the typical transient photoresponses of the In/MoS_2 synaptic device with 300 light pulses. A more detailed photo-response diagram is shown in Figure S10. Compared to the channel current generated from one light pulse, both the current and memory time of the In/MoS_2 synaptic device are increased significantly by applying more light pulses, which further demonstrates the existence of synaptic plasticity and functions of synaptic learning and memory. Figure 2g presents the corresponding synaptic weight variations at the different light pulse numbers and a voltage of 100 mV. The ΔEPSC value is increased from 4 to around 17 when the number of light pulses is increased from 1 to 300, revealing that the synaptic weights are adjustable. Moreover, to reach a current density of about 6 nA/cm^2, the voltage applied to the 55% In/MoS_2 synaptic device is 0.4 mV, which is much small than 320 mV of MoS_2 synaptic device without applying the indium layer. The typical transient photo-responses of the 55% In/MoS_2 synaptic device with 100 s illumination and 300 light pulses at a voltage of 0.4 mV are also characterized and the obtained results are shown in Figures S11a and S11b. The corresponding ΔEPSC values as functions of light duration time and number of light pulses are shown in Figures S11c and S11d, respectively. Results show that the synaptic device shows the synaptic plasticity and the synaptic strength can be enhanced at a very low voltage of 0.4 mV, which clearly demonstrate the low power consumption of this newly developed synaptic device.

In order to further explore the controllable functions of indium layer on MoS_2 synaptic devices, discontinuous indium layers with different coverage areas are deposited on MoS_2 films on the quartz substrate. The AFM images (Figures S12a-d) show that the indium layer becomes much thicker as the coverage of the indium layer is increased. To further clarify the coverage and morphology of the indium layers deposited with different evaporation times, the SEM images of indium layers deposited on MoS_2 film with different coverages are obtained and shown in Figure 3a. Similar to Figure 1d, the discontinuity of the indium layers can be clearly revealed from these SEM images. Furthermore, from Figure 3a (I-IV), both the coverage of the indium layer and the size of single indium islands deposited on the MoS_2 are gradually increased as the evaporation time of indium is increased. The coverage ratios of the indium layer extracted from Figure 3a as a function of evaporation time are shown in Figure 3b. If compared with the pillar-like structures of the indium layer on a pure quartz plate without MoS_2 (Figure S13a), the indium islands on the MoS_2 exhibit more regular shapes similar to a triangle or a hexagon, which is due to the epitaxial effect of the thermally evaporated indium on the MoS_2. Figure S13b shows the typical SEM images of the indium deposited on quartz and MoS_2, which obviously exhibit that the shapes of indium are quite different on pure quartz plate and MoS_2.

Figure 3c shows the corresponding channel currents (I_{ds}) as a function of applied voltage (V_{ds}) (output characteristics) of the MoS_2 synaptic devices deposited with the indium layers having different coverage ratios from 0 to 79%, without applying a gate voltage. An enlarged view of the output curves of the MoS_2 synaptic devices without and with 29% indium layer is shown in Figure S14. It should be noted that in order to compare the electrical properties, the thicknesses of MoS_2 films are maintained at the same value for the devices with and without an indium layer. An ohmic contact is formed between the layered MoS_2 film and the indium, which can be revealed from the linear voltage-current output curves. In addition, the conductivity of the channel is gradually increased with the increase of coverage ratio of the indium layer.

Compared with the MoS_2 synaptic device without the indium layer, the channel current of the 79% In/MoS_2 synaptic device has been increased up to about 1500 times under the same voltage. This remarkable enhancement in conductivities of synaptic devices is mainly due to the effective surface charge transfer doping between the indium layer and MoS_2. As the coverage ratio of the indium layer is increased, more electrons will be effectively transferred from the indium islands to MoS_2, thus making the MoS_2 more conductive. As a result, as the coverage of the indium layer is increased, a lower voltage is required to achieve a similar current density of the synaptic device. The corresponding source-drain voltages as a function of the indium coverage ratio with similar orders of magnitude of current densities are shown in Figure 3d. It is worthwhile to note that the voltage at a similar current density for the 79% In/MoS_2 synaptic device is 0.1 mV. However, due to the extremely weak electric field, the migration rate of the carriers is significantly reduced and the light-excited electron-hole pairs are easily recombined, thus resulting in the disappearance of light responses in this device. Therefore, a voltage of 0.4 mV is selected to apply to this 79% In/MoS_2 synaptic device. The fact that applied voltages can be adjusted by the coverage ratio of the indium layer once again proves the controllable surface charge transfer doping, which is effective for tuning the device's performance.

The capability of the indium layer to enhance the conductivity of the MoS_2 device can effectively reduce the power consumption of synaptic devices. As it is mentioned before, although many optically stimulated synaptic devices have been developed recently (Table S1), their power consumption readings are many times higher than that of the biological synapses, especially for those synaptic devices under an optical modulation, thus limiting the practical application of these devices. The power consumption of MoS_2 device developed in our work can be calculated by the formula of $E = I \times V \times t$, where I, V and t represent the response photocurrents, the applied reading voltage on devices, and the duration of light pulses, respectively. In order to compare the power consumption of MoS_2 devices with different coverage ratios of the indium layer, the performance of devices at the same current density is

investigated. Figures S15a-e show the current densities as a function of time under a light pulse (50 ms) for the MoS_2 synaptic devices deposited with different coverage ratios of the indium layer. The gradually decreasing voltages under the same magnitude of current density can effectively decrease the power consumption of the device. The corresponding power consumption readings per spike of the layered MoS_2 synaptic devices under different coverage ratios of the indium layer are shown in Figure 3d. Results show that the power consumption per spike can be reduced from 71.69 fJ to 68.9 aJ, which is much lower than the power consumption in biological synapses. A summary of power consumption results for all the reported artificial synaptic devices is shown in Figure 3e. It can be concluded that the power consumption for the In/MoS_2 device developed from this study is the lowest among all the optically stimulated synaptic devices reported so far.

Figures S16a-d show the dark currents, the currents after light illumination, the photocurrents and the ΔEPSC values under the light exposure for 100 s at 100 mV for the devices with different indium thicknesses. Figures S17a-d show the above mentioned four parameters obtained under the same testing conditions but with 300 light pulses. Introduction of the indium layer induces the surface charge transfer doping, which leads to the electrons in the indium layer effectively transferred into MoS_2. The more electrons are transferred into conduction band of MoS_2, the larger the dark current of In/MoS_2 synaptic device is. In the meantime, both the currents after light illumination and the photocurrent of synaptic device are increased. The ΔEPSC values of the MoS_2 synaptic devices with the indium layer are much lower than those of the MoS_2 synaptic devices without the indium layer, because the increase of the dark current is greater than the increased photocurrent. Therefore, by introducing an electron injection enhanced indium layer into MoS_2 synaptic devices in this study, the detection signals are significantly enhanced. Furthermore, five MoS_2 devices with various coverage ratios of the indium layers were fabricated. Their dark currents (Figure S18a) and currents after 5 s

light illumination (Figure S18b) show similar values, which demonstrates the uniformity of MoS_2 devices after applying the indium layer.

Inspired by the biological visual systems, a biomimetic eye based on In/MoS_2 synaptic devices is designed, fabricated and demonstrated. Its corresponding photographs are shown in Figure 4a. Figure 4b illustrates the corresponding detailed structures of the electronic biomimetic eye, which consist of a lens, a hemispherical shell and a hemispherical retina. The optical signals are focused by the lens and converted into electrical signals using the synaptic devices, thus realizing the visual perception and memory with a large field of view. As the central part, the artificial retina composed of a 5 × 5 In/MoS_2 synaptic devices array is directly fabricated on a hemispherical substrate. The fabrication process of the 5 × 5 In/MoS_2 synaptic device array on a hemispherical substrate is shown in Figure 4c. Firstly, the quartz hemisphere shell is covered with the MoS_2 film prepared using a two-step CVD method as shown in Figures S19a and S19b. This is different from the previous studies of hemispherical retina construction by simply transfering the device array constructed on a plane substrate to a hemispherical substrate.[4, 7, 9] Our method avoids the influences of wrinkles and defects (which are easily generated in the transfer process) on the photoelectric performance and improves the uniformity of devices. Moreover, the high-temperature resistant quartz hemispherical shells with a good light transparency are utilized as the substrates for depositing the MoS_2 films, which can enhance the performance. It is worthwhile to mention that the outer surface of the hemispheric shell is selected as the specific MoS_2 growth location in order to facilitate the wiring. The more fabrication details can be found in the experimental section. The insets in Figures S19a and S19b are the pictures of hemisphere shells before and after the MoS_2 deposition, respectively. It can be seen the hemispherical MoS_2 film has been successfully synthesized. With the aid of a PDMS mask obtained with the 3D printing technology (Figure S20), indium is thermally evaporated onto MoS_2 film. A method of depositing indium multiple times at different angles is adopted in this study, in order to make a uniform indium array deposited onto the curved

quartz substrate. The coresponding process is shown in Figures S21a-e and the picture of the indium array after all the evaporation processes is shown in Figure S21f.

Figure S22 shows the fabrication process of the electronic biomimetic eye. The customized acrylic sheets and PDMS are used to fix the hemispherical retinal array, which is connected with 25 copper wires through the silver paste. The electronic eye can be used for imaging after marking the serial number and fixing the copper wire. Figure 4d shows the images under either a dark condition or under illumination condition after different light durations without any masks. As the illumination time is increased, the current (normalized) of the In/MoS_2 synaptic device array is gradually increased, demonstrating the uniformity of the electronically biomimetic eye. It is worthwhile to note that the power consumption of the 5×5 In/MoS_2 synaptic devices array is about 1.42 fJ under the light illumination (with a wavelngth of 550 nm and a duration of 50 ms) at a voltage of 0.4 mV, which is about 20 times of the power consumption of a single In/MoS_2 synaptic device. This result is consistent with the relationship that the total power consumption in the circuit is nearly the sum of the power consumption of each device, further proving the ultra-low power consumption of a single In/MoS_2 synaptic device.

Figure 5a is the schematic structure of hemispherical electronic eye imaging process. The 5×5 In/MoS_2 synaptic device array can convert the light irradiated through the lens into electrical signals, forming a curved image reversed from the original image. The image sensing and learning functions of the letters H, I and T using the hemispherical electronic eye are shown in Figure 5b. When the light duration is increased from 10s to 100s, the letters H, I and T gradually become clearer and easier to be recognized. This is because the synaptic weight of In/MoS_2 synaptic device (normalized) is positively correlated with light exposure time, which means that the current of the 5×5 In/MoS_2 synaptic device array is much larger under a longer light duration than that under a shorter light duration. Therefore, the images can be learnt by the electronic eye through increasing the light illumination durations. Furthermore, to

demonstrate image memory functions of the hemispherical electronic eye, the images of the letters H, I and T, which are illuminated for 100 s and then left for different durections of 10 s, 50 s (Figure S23) and 100 s (Figure 5b), are taken and compared. With the increase of durations after switching off the light illumination, the images become slowly and gradually blurred. This is mainly due to the slow combination process of photogenerated electron-hole pairs, thus resulting in the gradual decrease of the current. Waiting for 100 s after the light illumination (for 100 s) is switched off, the measured current value of the illumintaed devices is still maintained at ~42% of the current value (which is measured right after switching off the illumination). Moreover, the images of different letters can still be distinguished after 100 s, demonstrating that the fabricated hemispherical electronic eye based imaging system has shown the excellent image memory function. The images of the letters H, I and T without any light illumination are shown in Figure S24. The uniform color distribution in the images proves the uniformity of dark currents in MoS_2 synaptic devices. Moreover, there are clear images of letters observed after applying illumination, whereas no images are formed when not using the light illumination. Results clearly demonstrate the imaging capabilities of the hemispherical electronic eye under the light illumination.

In summary, we present an artificial optical synapse device based on MoS_2 with an indium layer for enhanced electrons injection. The electrons in the indium layer can be effectively transferred into the MoS_2 film, thus improving the channel conductivity and decreasing the power consumption of the MoS_2 synaptic devices. The ultralow power consumption of 68.9 aJ per spike is much lower than those of other optical synapse devices, which is of great significance for the practical applications. Synaptic plasticities including STP, LTP and their transitions between them can be simulated using this In/MoS_2 optical synapse device. Moreover, a 5 × 5 array of In/MoS_2 synaptic device is constructed to form a hemispherical electronic retina and shows the capabilities of image sensing and learning. This work will inspire new ideas for

the artificial vision systems, opening up a new path for research in biomimetic synapses and eyes.

Experimental Section

Synthesis of MoS_2 film: A CVD method was used to synthesis the MoS_2 film on quartz plates. An alumina boat loaded with 500 mg of sulfur powder was placed at the upstream heating center in a quartz tube. Firstly, 10 mg $(NH_4)_2Mo_4O_{13}\cdot 2H_2O$ (Aladdin, 99%) were placed in an alumina boat with a quartz plate at the downstream heating center of a quartz tube.

A two-step CVD method was applied to synthesis MoS_2 film on the hemispherical quartz substrates. The customized hemispherical quartz substrates (20 mm in diameter and 1 mm thick) were ultrasonically cleaned with acetone, isopropanol and ethanol in a sequence. The first step was to synthesize MoS_2 films on the ceter part of the quartz hemispherical shell using the same CVD process. Next, to synthesize the MoS_2 film on the edge area of the quartz hemisphere shell, the quartz hemispherical shell was buckled down on a graphite plate and evenly surrounded by 40 mg $(NH_4)_2Mo_4O_{13}\cdot 2H_2O$ powders.

During these CVD processes, the downstream heating center was ramped up to 750 °C and maintained for 20 min. The sulfur powders at the upstream heating center were heated to 250 °C when the quartz plates or quartz hemispherical shell substrates were heated to 750 °C with 30 sccm flow of argon gas at an atmospheric pressure. Then the furnace was cooled down naturally to room temperature and MoS_2 film on quartz plate or wrapped in a quartz hemispherical shell was synthesized.

Characterization: As the MoS_2 film on the quartz hemispherical shell was difficult to perform various characterizations, we used the same method (as used in the first step) in the two-step method to prepare a flat MoS_2 film on the quartz plate for characterization. Raman and photoluminescence (PL) spectra were collected using a confocal Raman spectroscope (LabRAM XploRA) with a 532 nm laser as the excitation source. The SEM images were

acquired by using a Hitachi SU-8010 microscope. AFM (Dimension Icon, Bruker) was carried out to probe the thickness of the samples. XRD (Diffractometer-6000, Cu Kα radiation, λ = 0.1542 nm) was used to characterize the structure of MoS_2. XPS (Thermo Scientific K-alpha XPS, using Al (Kα) radiation as a probe) was used to characterize the chemical composition and bonding structures of the as-grown MoS_2 sample. TEM (Tacnai-G2 F30) was performed to determine the internal microstructure of MoS_2. MoS_2 films were transferred onto a copper grid for TEM characterization.

Device fabrication and measurement: The hemispherical electronic eye consisting of MoS_2 synaptic device array was fabricated by thermal evaporating a top layer of an indium film. The corresponding mask in the thermal evaporation process was constructed by using a complementary PDMS socket with 5 × 5 hole array (square hole size 2 × 2 mm), which was obtained using a 3D printing technology. Then the devices were thermally annealed at 150 ℃ for 30 min to minimize the effects of physisorbed oxygen and water on the surface. After that, 25 copper wires were connected to the In/MoS_2 synaptic device using the silver paste. Acrylic boards and PDMS were used to fix and package this hemispherical electronic eye. The optoelectronic characterization of MoS_2 synaptic devices was performed using a Keithley 4200-SCS Parameter Analyzer. The laser applied to devices was carried out using a xenon lamp and a monochromator (Zolix, Omni-λ300i). A power meter (Thorlabs, PM100D) was used to measure the corresponding light power density. All the measurements were performed at the atmospheric pressure and room temperature. In each pixel of the hemispherical electronic eye, the length of the channel was about 1.1 mm and the width of the channel was about 0.4 mm for each device. The pixel was illuminated and measured one by one, and the pixel current was obtained sequentially.

Supporting Information

Supporting Information is available from the Wiley Online Library or from the author.

Acknowledgements
This work is supported by National Basic Research Program of China (2019YFB1310200), Foundation for Innovative Research Groups of the National Natural Science Foundation of China (NSFC no. 51521003), Self-Planned Task of State Key Laboratory of Robotics and System (HIT) (no. SKLRS201801B), as well as Newton Mobility Grant (IE161019) and International Exchange Grant (IEC/NSFC/201078) through Royal Society and NFSC.

Received: ((will be filled in by the editorial staff))
Revised: ((will be filled in by the editorial staff))
Published online: ((will be filled in by the editorial staff))

References

[1] M. S. Humayun, E. de Juan, *Eye* **1998**, *12*, 605.

[2] E. K. Lee, R. K. Baruah, J. W. Leem, W. Park, B. H. Kim, A. Urbas, Z. Ku, Y. L. Kim, M. A. Alam, C. H. Lee, *Adv Mater* **2020**, *32*, e2004456.

[3] G. J. Lee, C. Choi, D.-H. Kim, Y. M. Song, *Adv. Funct. Mater.* **2018**, *28*, 1705202.

[4] C. Choi, M. K. Choi, S. Liu, M. S. Kim, O. K. Park, C. Im, J. Kim, X. Qin, G. J. Lee, K. W. Cho, M. Kim, E. Joh, J. Lee, D. Son, S.-H. Kwon, N. L. Jeon, Y. M. Song, N. Lu, D.-H. Kim, *Nat. Commun.* **2017**, *8*, 1664.

[5] L. Gu, S. Poddar, Y. Lin, Z. Long, D. Zhang, Q. Zhang, L. Shu, X. Qiu, M. Kam, A. Javey, Z. Fan, *Nature* **2020**, *581*, 278.

[6] D. Floreano, R. Pericet-Camara, S. Viollet, F. Ruffier, A. Bruckner, R. Leitel, W. Buss, M. Menouni, F. Expert, R. Juston, M. K. Dobrzynski, G. L'Eplattenier, F. Recktenwald, H. A. Mallot, N. Franceschini, *Proc. Natl. Acad. Sci. U.S.A.* **2013**, *110*, 9267.

[7] H. C. Ko, M. P. Stoykovich, J. Song, V. Malyarchuk, W. M. Choi, C. J. Yu, J. B. Geddes, 3rd, J. Xiao, S. Wang, Y. Huang, J. A. Rogers, *Nature* **2008**, *454*, 748.

[8] F. Zhou, Z. Zhou, J. Chen, T. H. Choy, J. Wang, N. Zhang, Z. Lin, S. Yu, J. Kang, H. S. P. Wong, Y. Chai, *Nat. Nanotechnol.* **2019**, *14*, 776.

[9] K. Zhang, Y. H. Jung, S. Mikael, J.-H. Seo, M. Kim, H. Mi, H. Zhou, Z. Xia, W. Zhou, S. Gong, Z. Ma, *Nat. Commun.* **2017**, *8*, 1782.

[10] T. Ahmed, S. Kuriakose, E. L. H. Mayes, R. Ramanathan, V. Bansal, M. Bhaskaran, S. Sriram, S. Walia, *Small* **2019**, *15*, 1900966.

[11] T. Ahmed, M. Tahir, M. X. Low, Y. Ren, S. A. Tawfik, E. L. H. Mayes, S. Kuriakose, S. Nawaz, M. J. S. Spencer, H. Chen, M. Bhaskaran, S. Sriram, S. Walia, *Adv. Mater.* **2021**, *33*, 2004207.

[12] S. H. Jo, T. Chang, I. Ebong, B. B. Bhadviya, P. Mazumder, W. Lu, *Nano Lett.* **2010**, *10*, 1297.

[13] W. Qiu, Y. Huang, L.-A. Kong, Y. Chen, W. Liu, Z. Wang, J. Sun, Q. Wan, J. H. Cho, J. Yang, Y. Gao, *Adv. Funct. Mater.* **2020**, *30*, 2002325.

[14] Q. Wu, J. Wang, J. Cao, C. Lu, G. Yang, X. Shi, X. Chuai, Y. Gong, Y. Su, Y. Zhao, N. Lu, D. Geng, H. Wang, L. Li, M. Liu, *Adv. Electron. Mater.* **2018**, *4*, 1800556.

[15] S. Dai, X. Wu, D. Liu, Y. Chu, K. Wang, B. Yang, J. Huang, *ACS Appl. Mater. Interfaces* **2018**, *10*, 21472.

[16] Y. X. Hou, Y. Li, Z. C. Zhang, J. Q. Li, D. H. Qi, X. D. Chen, J. J. Wang, B. W. Yao, M. X. Yu, T. B. Lu, J. Zhang, *ACS Nano* **2021**, *15*, 1497.

[17] L. Wang, W. Liao, S. L. Wong, Z. G. Yu, S. Li, Y. F. Lim, X. Feng, W. C. Tan, X. Huang, L. Chen, L. Liu, J. Chen, X. Gong, C. Zhu, X. Liu, Y. W. Zhang, D. Chi, K. W. Ang, *Adv. Funct. Mater.* **2019**, *29*.

[18] Z. P. Ling, R. Yang, J. W. Chai, S. J. Wang, W. S. Leong, Y. Tong, D. Lei, Q. Zhou, X. Gong, D. Z. Chi, K. W. Ang, *Opt. Express* **2015**, *23*, 13580.

[19] W. Zhang, J.-K. Huang, C.-H. Chen, Y.-H. Chang, Y.-J. Cheng, L.-J. Li, *Adv. Mater.* **2013**, *25*, 3456.

[20] H.-Y. Chang, S. Yang, J. Lee, L. Tao, W.-S. Hwang, D. Jena, N. Lu, D. Akinwande, *ACS Nano* **2013**, *7*, 5446.

[21] M. Dai, W. Zheng, X. Zhang, S. Wang, J. Lin, K. Li, Y. Hu, E. Sun, J. Zhang, Y. Qiu, Y. Fu, W. Cao, P. Hu, *Nano Lett.* **2020**, *20*, 201.

[22] W. Zheng, J. Lin, W. Feng, K. Xiao, Y. Qiu, X. Chen, G. Liu, W. Cao, S. T. Pantelides, W. Zhou, P. Hu, *Adv. Funct. Mater.* **2016**, *26*, 6371.

[23] J. Zhu, H. Xu, G. Zou, W. Zhang, R. Chai, J. Choi, J. Wu, H. Liu, G. Shen, H. Fan, *JACS* **2019**, *141*, 5392.

[24] X. Song, Z. Guo, Q. Zhang, P. Zhou, W. Bao, D. W. Zhang, *Small* **2017**, *13*, 1700098.

[25] P. Yang, X. Zou, Z. Zhang, M. Hong, J. Shi, S. Chen, J. Shu, L. Zhao, S. Jiang, X. Zhou, Y. Huan, C. Xie, P. Gao, Q. Chen, Q. Zhang, Z. Liu, Y. Zhang, *Nat. Commun.* **2018**, *9*, 979.

[26] Y. Hu, M. Dai, W. Feng, X. Zhang, S. Zhang, B. Tan, H. Shang, *Mater. Horizons* **2020**, *7*, 3316.

[27] W. Wang, S. Gao, Y. Li, W. Yue, H. Kan, C. Zhang, Z. Lou, L. Wang, G. Shen, *Adv. Funct. Mater.* **2021**, *n/a*, 2101201.

[28] S. Wang, C. Chen, Z. Yu, Y. He, X. Chen, Q. Wan, Y. Shi, D. W. Zhang, H. Zhou, X. Wang, P. Zhou, *Adv. Mater.* **2019**, *31*, 1806227.

[29] J. J. Nassi, E. M. Callaway, *Nat. Rev. Neurosci.* **2009**, *10*, 360.

[30] D. Wang, Y. Zhou, H. Zhang, R. Zhang, H. Dong, R. Xu, Z. Cheng, Y. He, Z. Wang, *Inorg. Chem.* **2020**, *59*, 17356.

[31] Q. Ji, Y. Zhang, T. Gao, Y. Zhang, D. Ma, M. Liu, Y. Chen, X. Qiao, P.-H. Tan, M. Kan, J. Feng, Q. Sun, Z. Liu, *Nano Lett.* **2013**, *13*, 3870.

[32] J. Lee, S. Pak, P. Giraud, Y.-W. Lee, Y. Cho, J. Hong, A. R. Jang, H.-S. Chung, W.-K. Hong, H. Y. Jeong, H. S. Shin, L. G. Occhipinti, S. M. Morris, S. Cha, J. I. Sohn, J. M. Kim, *Adv. Mater.* **2017**, *29*, 1702206.

[33] H.-K. He, R. Yang, W. Zhou, H.-M. Huang, J. Xiong, L. Gan, T.-Y. Zhai, X. Guo, *Small* **2018**, *14*, 1800079.

[34] A. Di Bartolomeo, L. Genovese, T. Foller, F. Giubileo, G. Luongo, L. Croin, S.-J. Liang, L. K. Ang, M. Schleberger, *Nanotechnology* **2017**, *28*, 214002.

[35] X. Li, M.-W. Lin, A. A. Puretzky, L. Basile, K. Wang, J. C. Idrobo, C. M. Rouleau, D. B. Geohegan, K. Xiao, *J. Mater. Res.* **2016**, *31*, 923.

[36] P. Ci, X. Tian, J. Kang, A. Salazar, K. Eriguchi, S. Warkander, K. Tang, J. Liu, Y. Chen, S. Tongay, W. Walukiewicz, J. Miao, O. Dubon, J. Wu, *Nat. Commun.* **2020**, *11*, 5373.

[37] Y. Cheng, Y. Chang, Y. Feng, H. Jian, Z. Tang, H. Zhang, *Angew Chem. Int. Ed. Engl.* **2018**, *57*, 246.

[38] N. Ma, K. Zhang, Y. Yang, *Adv. Mater.* **2017**, *29*, 1703694.

[39] K. Zhang, S. Wang, Y. Yang, *Adv. Energy Mater.* **2017**, *7*, 1601852.

[40] X. Yan, Q. Zhao, A. P. Chen, J. Zhao, Z. Zhou, J. Wang, H. Wang, L. Zhang, X. Li, Z. Xiao, K. Wang, C. Qin, G. Wang, Y. Pei, H. Li, D. Ren, J. Chen, Q. Liu, *Small* **2019**, *15*, 1901423.

[41] D. Debanne, N. C. Guérineau, B. H. Gähwiler, S. M. Thompson, *J. Physiol.* **1996**, *491*, 163.

[42] R. A. John, F. Liu, N. A. Chien, M. R. Kulkarni, C. Zhu, Q. Fu, A. Basu, Z. Liu, N. Mathews, *Adv. Mater.* **2018**, *30*, 1800220.

[43] M. Li, C.-Y. Lin, S.-H. Yang, Y.-M. Chang, J.-K. Chang, F.-S. Yang, C. Zhong, W.-B. Jian, C.-H. Lien, C.-H. Ho, H.-J. Liu, R. Huang, W. Li, Y.-F. Lin, J. Chu, *Adv. Mater.* **2018**, *30*, 1803690.

[44] Y.-T. Huang, Y.-H. Chen, Y.-J. Ho, S.-W. Huang, Y.-R. Chang, K. Watanabe, T. Taniguchi, H.-C. Chiu, C.-T. Liang, R. Sankar, F.-C. Chou, C.-W. Chen, W.-H. Wang, *ACS Appl. Mater. Interfaces* **2018**, *10*, 33450.

[45] C. Kim, I. Moon, D. Lee, M. S. Choi, F. Ahmed, S. Nam, Y. Cho, H.-J. Shin, S. Park, W. J. Yoo, *ACS Nano* **2017**, *11*, 1588.

[46] R. C. Atkinson, R. M. Shiffrin, in *Psychology of Learning and Motivation*, Vol. 2, Elsevier, London **1968**, p. 89.

[47] W. Schneider, M. Detweiler, in *Psychology of Learning and Motivation*, Vol. 21, Elsevier, London **1988**, p. 53.

[48] H. Tan, Z. Ni, W. Peng, S. Du, X. Liu, S. Zhao, W. Li, Z. Ye, M. Xu, Y. Xu, X. Pi, D. Yang, *Nano Energy* **2018**, *52*, 422.

[49] T.-Y. Wang, J.-L. Meng, Z.-Y. He, L. Chen, H. Zhu, Q.-Q. Sun, S.-J. Ding, P. Zhou, D. W. Zhang, *Adv. Sci.* **2020**, *7*, 1903480.

[50] Y. Wang, J. Yang, Z. Wang, J. Chen, Q. Yang, Z. Lv, Y. Zhou, Y. Zhai, Z. Li, S.-T. Han, *Small* **2019**, *15*, 1805431.

[51] L. Chen, T. Y. Wang, Y. W. Dai, M. Y. Cha, H. Zhu, Q. Q. Sun, S. J. Ding, P. Zhou, L. Chua, D. W. Zhang, *Nanoscale* **2018**, *10*, 15826.

[52] A. Kurenkov, S. DuttaGupta, C. Zhang, S. Fukami, Y. Horio, H. Ohno, *Adv. Mater.* **2019**, *31*, 1900636.

[53] C. S. Yang, D. S. Shang, N. Liu, G. Shi, X. Shen, R. C. Yu, Y. Q. Li, Y. Sun, *Adv. Mater.* **2017**, *29*, 1700906.

[54] J. Zhu, Y. Yang, R. Jia, Z. Liang, W. Zhu, Z. U. Rehman, L. Bao, X. Zhang, Y. Cai, L. Song, R. Huang, *Adv. Mater.* **2018**, *30*, 1800195.

[55] B. Tian, L. Liu, M. Yan, J. Wang, Q. Zhao, N. Zhong, P. Xiang, L. Sun, H. Peng, H. Shen, T. Lin, B. Dkhil, X. Meng, J. Chu, X. Tang, C. Duan, *Adv. Electron. Mater.* **2019**, *5*, 1800600.

[56] X. Feng, Y. Li, L. Wang, S. Chen, Z. G. Yu, W. C. Tan, N. Macadam, G. Hu, L. Huang, L. Chen, X. Gong, D. Chi, T. Hasan, A. V.-Y. Thean, Y.-W. Zhang, K.-W. Ang, *Adv. Electron. Mater.* **2019**, *5*, 1900740.

[57] T. Paul, T. Ahmed, K. Kanhaiya Tiwari, C. Singh Thakur, A. Ghosh, *2D Mater.* **2019**, *6*, 045008.

[58] C. Zhang, S. Wang, X. Zhao, Y. Yang, Y. Tong, M. Zhang, Q. Tang, Y. Liu, *Adv. Funct. Mater.* **2021**, *31*, 2007894.

[59] H. K. He, R. Yang, H. M. Huang, F. F. Yang, Y. Z. Wu, J. Shaibo, X. Guo, *Nanoscale* **2020**, *12*, 380.

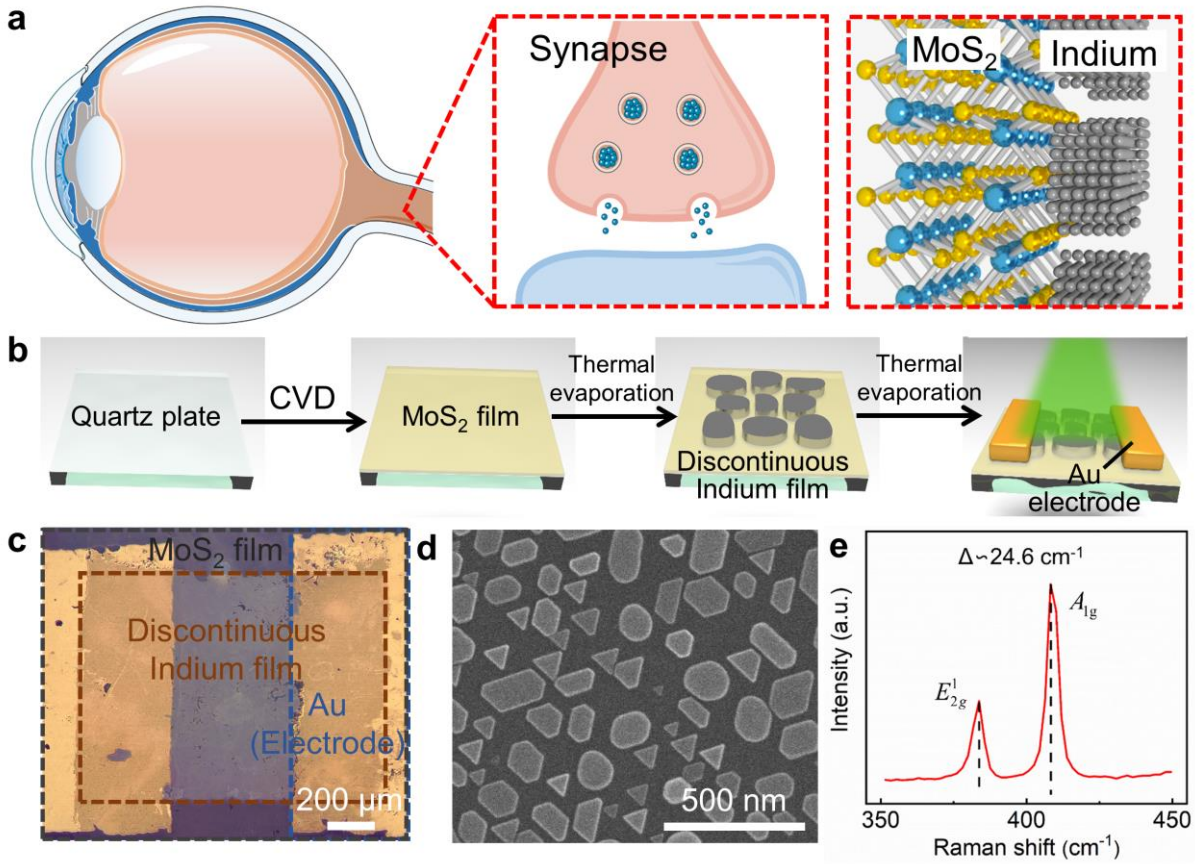

Figure 1. MoS_2 synaptic devices deposited by indium islands. a) Schematic of the human eye, the biological synapse and the structure of In/MoS_2 synaptic device. b) Schematic of In/MoS_2 synaptic device fabrication process. c) An optical microscope photograph of a representative In/MoS_2 synaptic device. d) The SEM image of indium islands on MoS_2 film. e) Raman spectrum of as-synthesized multilayer MoS_2 film.

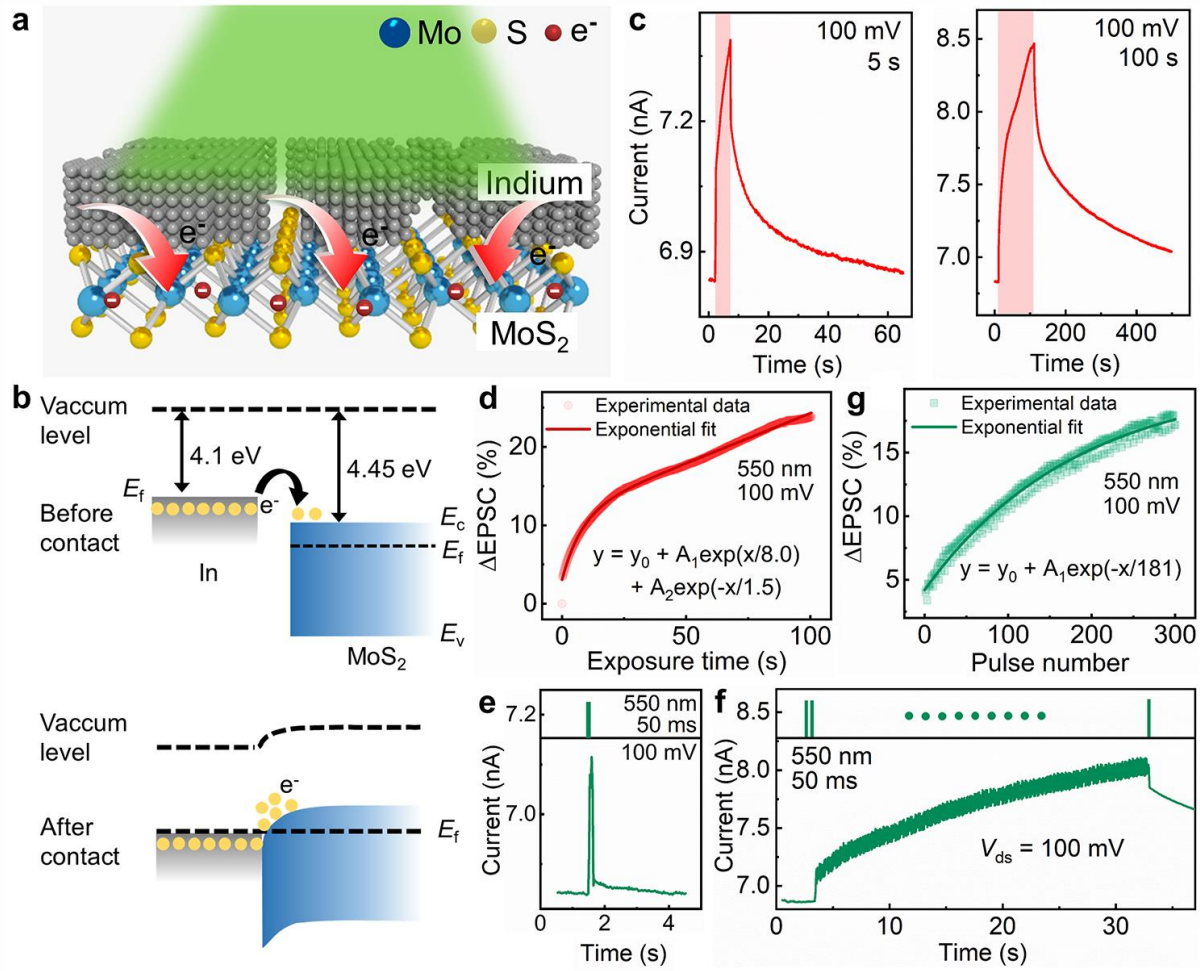

Figure 2. Optoelectronic properties of In/MoS_2 synaptic devices. a) Schematic illustration of the surface charge doping procedure in In/MoS_2 synaptic device. b) Schematic diagram of energy band structure before and after indium layer deposition on layered MoS_2. c) The emulation of STP and LTP phenomenon by different duration times of 5 s and 100 s under 550 nm wavelength at intensity of 23.6 mW•cm^{-2} of 100 mV. d) Change in synaptic weight (ΔEPSC) as a function of duration under 550 nm wavelength with power intensity of 23.6 mW•cm^{-2} at a voltage of 100 mV. Typical transient photoresponse of the In/MoS_2 synaptic devices with e) one light pulse (pulse width of 50 ms, pulse interval of 50 ms) and f) 300 light pulses under 550 nm wavelength with power intensity of 23.6 mW•cm^{-2} at a voltage of 100 mV. g) ΔEPSC as a function the numbers of light pulses at 100 mV.

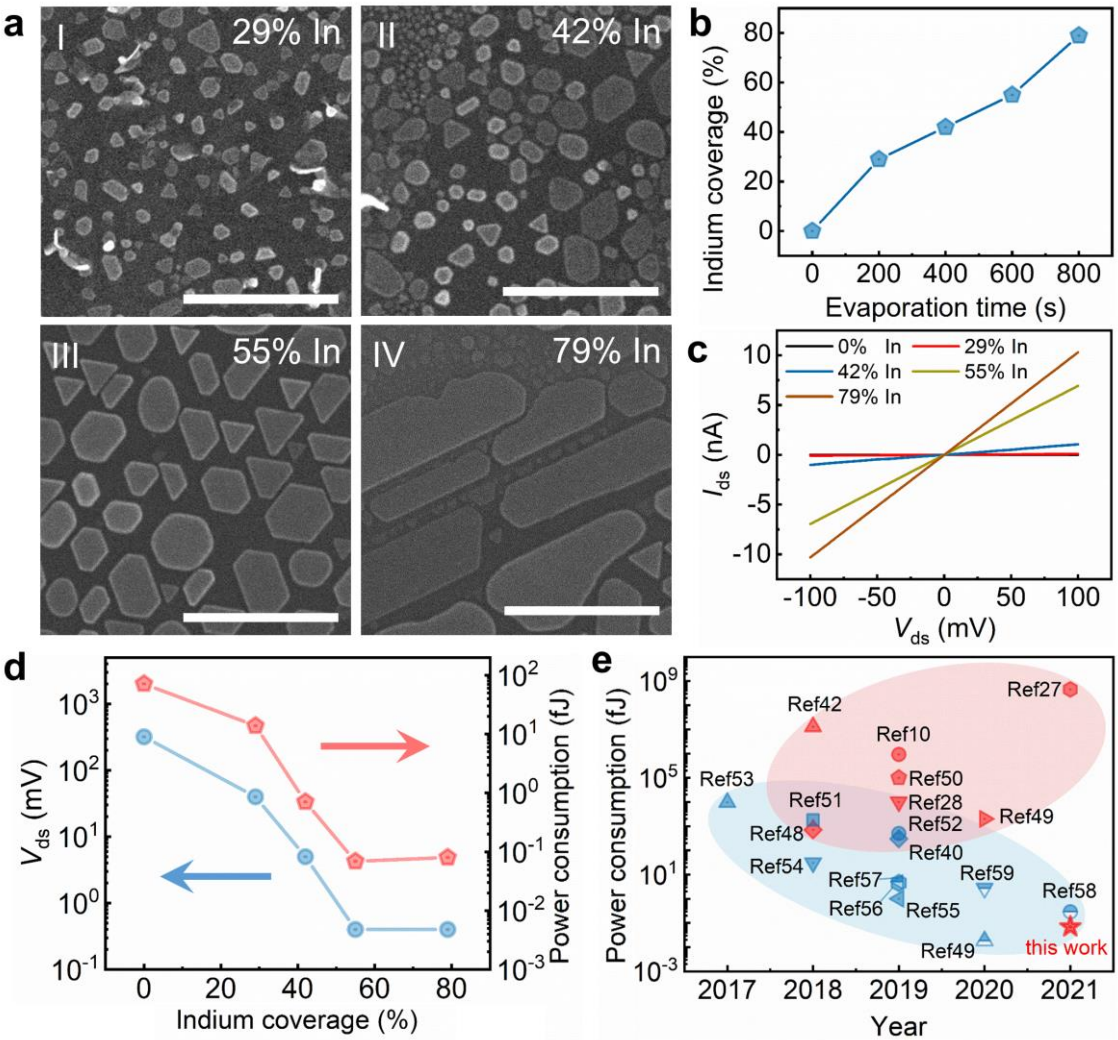

Figure 3. In/MoS_2 synaptic devices with different indium coverage. a) SEM images on MoS_2 film with I: 29%; II: 42%; III: 55% and IV: 79% indium coverage. The scale bar is 500 nm. b) Indium coverage as a function of evaporation time. c) Output characteristics of MoS_2 synaptic devices with various indium coverage from 0% to 79%. d) The variation of source-drain voltages and power consumption of layered MoS_2 synaptic devices as a function of indium coverage when the current densities of MoS_2 synaptic devices are at the same order of magnitude. e) Power consumption summary of artificial synaptic devices.

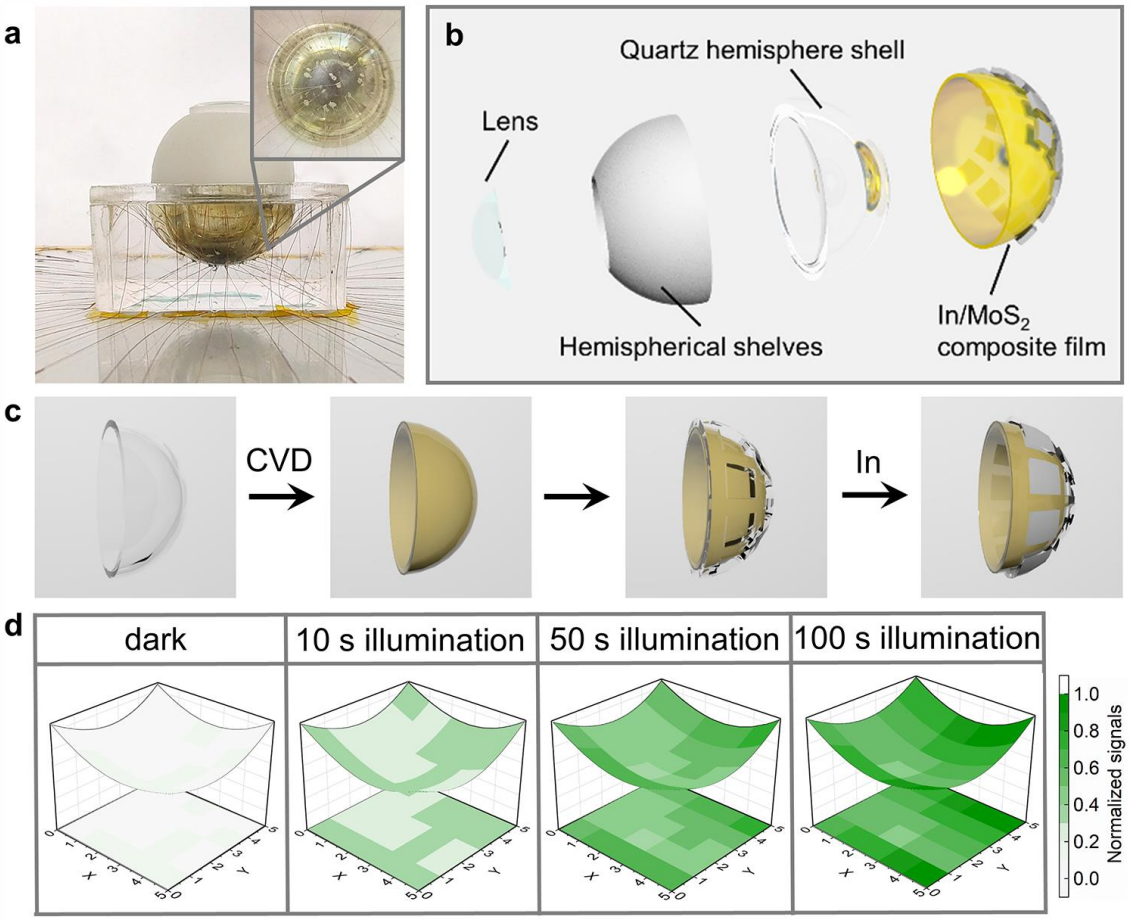

Figure 4. The fabrication of a hemispherical synaptic device array. a) Photographs of our hemispherical electronic eye. b) Exploded view of electronic eye. c) The fabrication process of the indium array on MoS_2 hemisphere. d) Illustrations of the imaging functions under dark condition, 10 s, 50 s and 100 s with light wavelength of 550 nm and light intensity of 23.6 mW•cm^{-2} at a voltage of 0.4 mV without masks, respectively.

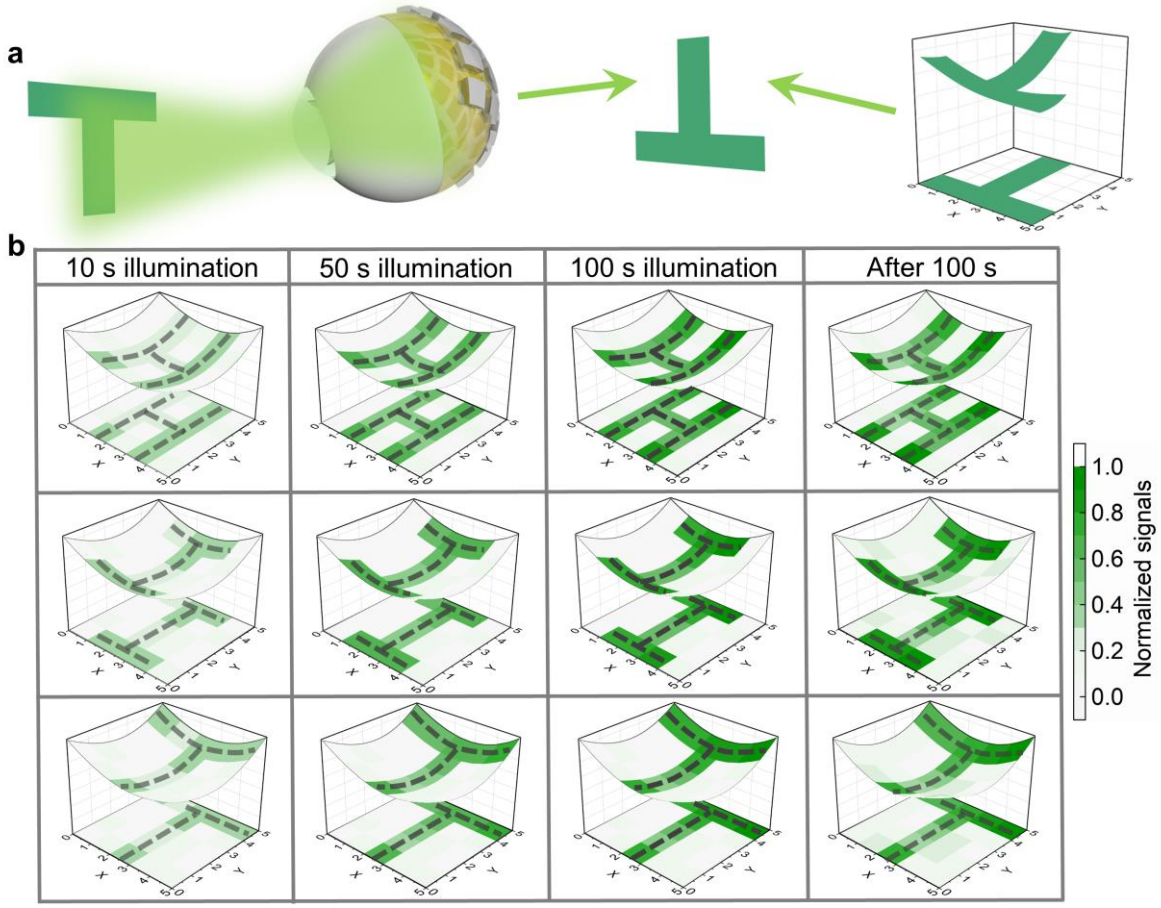

Figure 5. Image learning function of our biomimetic eye. a) Schematic structure of hemispherical electronic eye imaging system consisting of a 5 × 5 MoS_2 synaptic devices array. b) Illustrations of the imaging function of the letter H, I and T under 10 s, 50 s and 100 s illumination and for waiting 100 s after 100 s illumination with light wavelength of 550 nm and light intensity of 23.6 mW•cm^{-2} at a voltage of 0.4 mV, respectively.

By introducting electron injection enhancement layers of indium, a synaptic device of In/MoS_2 show ultra-low power consumption of 68.9 aJ, short-term plasticity (STP) and long-term plasticity (LTP), good capability of transition between STP and LTP. Additionally, a biomimetic eye with a 5 × 5 array of In/MoS_2 synaptic devices has been implemented and exhibited excellent image sensing and learning functions.

Keywords: synaptic devices, MoS_2, ultra-low power consumption, biomimetic eyes, image learning

Y. Hu, M. Dai, W. Feng, X. Zhang, F. Gao, S. Zhang, B. Tan, J. Zhang, Y. Shuai, Y.Q. Fu, P. Hu*

Ultra-low power optical synapses based on MoS_2 layers with indium-induced surface charge doping for biomimetic eyes

ToC figure